AD-7/GBAR status report for the 2024 CERN SPSC

February 2, 2024

P. Adrich[1], P. Blumer[2], G. Caratsch[2], M. Chung[3], P. Cladé[4], P. Comini[5], P. Crivelli[2], O. Dalkarov[6], P. Debu[5], A. Douillet[4,7], D. Drapier[4], P. Froelich[8,21], N. Garroum[4,22], S. Geffroy[15], S. Guellati-Khelifa[4,9], J. Guyomard[4], P-A. Hervieux[10], L. Hilico[4,7], P. Indelicato[4], S. Jonsell[8], J-P. Karr[4,7], B. Kim[11], S. Kim[12], E-S. Kim[13], Y.J. Ko[11], T. Kosinski[1], N. Kuroda[14], B.M. Latacz[5,23], B. Lee[12], H. Lee[12], J. Lee[11], E. Lim[13], L. Liszkay[5], D. Lunney[15], G. Manfredi[10], B. Mansoulié[5], M. Matusiak[1], V. Nesvizhevsky[16], F. Nez[4], S. Niang[15,23], B. Ohayon[2], K. Park[11,12], N. Paul[4], P. Pérez[5], C. Regenfus[2], S. Reynaud[4], C. Roumegou[15], J-Y. Roussé[5], Y. Sacquin[5], G. Sadowski[5], J. Sarkisyan[2], M. Sato[14], F. Schmidt-Kaler[17], M. Staszczak[1], K. Szymczyk[1], T.A. Tanaka[14], B. Tuchming[5], B. Vallage[5], A. Voronin[6], D.P. van der Werf[18], A. Welker[19,24], D. Won[12], S. Wronka[1], Y. Yamazaki[20], K-H. Yoo[3], P. Yzombard[4]

(GBAR Collaboration)

[1] *National Centre for Nuclear Research (NCBJ), ul. Andrzeja Soltana 7, 05-400 Otwock, Swierk, Poland*
[2] *Institute for Particle Physics and Astrophysics, ETH Zurich, 8093 Zurich, Switzerland*
[3] *Department of Physics, Ulsan National Institute of Science and Technology (UNIST), 50, UNIST-gil, Ulsan 44919, Republic of Korea*
[4] *Laboratoire Kastler Brossel, Sorbonne Université, CNRS, ENS-Université PSL, Collège de France, Campus Pierre et Marie Curie, 4, place Jussieu, F-75005 Paris, France*
[5] *IRFU, CEA, Université Paris-Saclay, F-91191 Gif-sur-Yvette, France*
[6] *Affiliated with an institute covered by a cooperation agreement with CERN*
[7] *Université d'Evry-Val d'Essonne, Université Paris-Saclay, Boulevard François Mitterand, F-91000 Evry, France*
[8] *Department of Physics, Stockholm University, SE-10691 Stockholm, Sweden*
[9] *Conservatoire National des Arts et Métiers, 292 rue Saint Martin, 75003 Paris, France*
[10] *Université de Strasbourg, CNRS, Institut de Physique et Chimie des Matériaux de Strasbourg, UMR 7504, F-67000 Strasbourg, France*
[11] *Center for Underground Physics, Institute for Basic Science, 70 Yuseong-daero 1689-gil, Yuseong-gu, Daejeon 34047, Korea*
[12] *Department of Physics and Astronomy, Seoul National University, 1 Gwanak-Ro, Gwanak-gu, Seoul 08826, Korea*
[13] *Department of Accelerator Science, Korea University Sejong Campus, Sejong-ro 2511, 30019 Sejong, Republic of Korea*
[14] *Institute of Physics, University of Tokyo, 3-8-1 Komaba, Meguro, Tokyo 153-8902, Japan*
[15] *Université Paris-Saclay, CNRS/IN2P3, IJCLab, Orsay, France*
[16] *Institut Max von Laue - Paul Langevin (ILL), 71 avenue des Martyrs, Grenoble, France, F-38042*
[17] *QUANTUM, Institut für Physik, Johannes Gutenberg Universität, D-55128 Mainz, Germany*
[18] *Department of Physics, Faculty of Science and Engineering, Swansea University, Swansea SA2 8PP, United Kingdom*
[19] *CERN, Esplanade des Particules 1, 1217 Meyrin, Switzerland*
[20] *Ulmer Fundamental Symmetries Laboratory, RIKEN, 2-1 Hirosawa, Wako, 351-0198, Saitama, Japan*
[21] *Present address, Uppsala University, Angstrom Laboratory, Department of Chemistry, Box 523, 75120 Uppsala, Sweden*
[22] *Present address, LPNHE/IN2P3, 4, place Jussieu, 75252 Paris, France*
[23] *Present address, CERN, Esplanade des Particules 1, 1217 Meyrin, Switzerland*
[24] *Present address, 6300, Zug, Switzerland*

CERN-SPSC-2024-006 / SPSC-SR-341
03/02/2024

Abstract

We report on the activities performed during 2023 and the plans for 2024 for the GBAR experiment.

1 Introduction

The year 2023 was marked by three major milestones: first the publication of an article based on the data taken in 2022, demonstrating the production of antihydrogen atoms in GBAR, second on the positron line, the replacement of one stage of buffer gas trapping by a SiC remoderator, third on the antiproton line, the installation of the antiproton trap in its nominal position, after the decelerating drift tube and before the reaction chamber.

Figure 1 shows the most recent configuration of the experiment. Namely the positron beam produced with a linac followed by two traps for e^+ accumulation, the antiproton beam delivered by ELENA being further decelerated with the pulsed-drift-tube, followed by the antiproton trap. The beams from the high field positron trap and from the antiproton trap are focused to the same

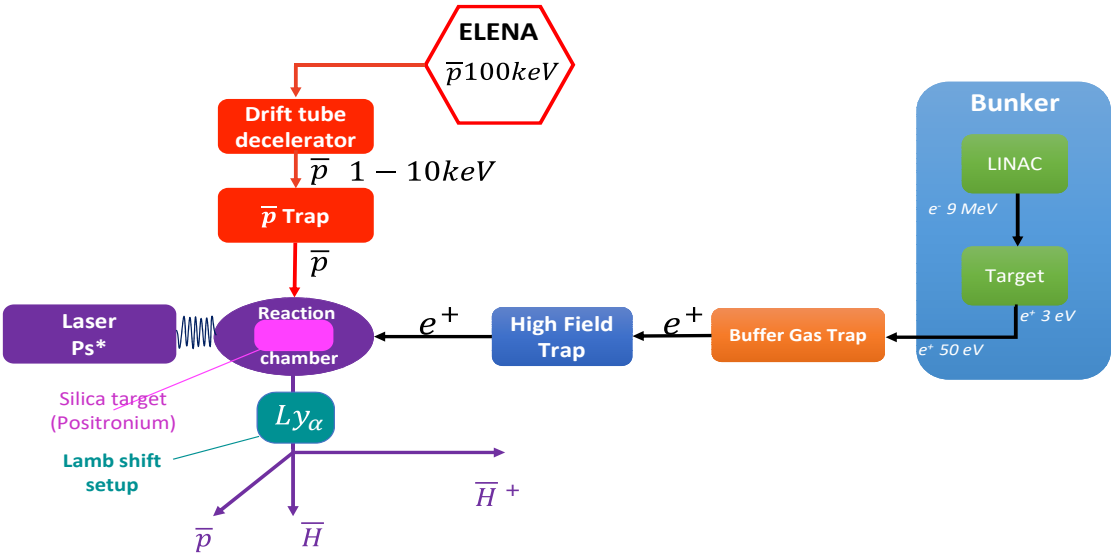

Figure 1: *Scheme of the present version of the GBAR experiment.*

point where positrons are converted into positronium (Ps), which can be excited using a laser pulse. Antihydrogen atoms travel to a dedicated setup to measure their Lamb shift. The outgoing charged particles are separated employing an electrostatic switchyard.

2 Article on antihydrogen production in GBAR

In 2022, for the first time in GBAR, antiprotons from ELENA, decelerated to 6 keV were sent onto a positronium cloud produced in the reaction chamber by positrons impinging on a flat target of porous silica. The experimental procedure was reported in the 2023 SPSC report. The complete analysis of these data was published in 2023 in an article in EPJC [1]. Here we briefly summarize the results. About 7000 antiproton spills from ELENA were used in conjunction with a Ps cloud, and about 8500 spills were used without Ps cloud. For each spill, the average number of antiprotons entering the cloud was 3.07×10^6, the number of positrons impinging on the converter was 3.9×10^7, the e^+-to- Ps conversion efficiency was 0.18, the cross-section area of the $\overline{p}$-cloud intersection region was 0.2 cm^2. Considering all the "mixing" spills, about 20 excess events attributed to antihydrogen formation were observed on top of a background of about 15 events, providing a 3.1 standard

deviation evidence. The production rate is in rough agreement with theoretical expectations for the cross section of the reaction $\overline{\mathrm{p}}+\mathrm{Ps} \rightarrow \overline{\mathrm{H}}$, but due to uncertainties in the $\overline{\mathrm{H}}$ detection acceptance, only a lower limit of the cross-section value could be established.

3 Positron production and trapping

The linac klystron was replaced in January 2023 with a second-hand unit purchased from Tesla Systems Research, Inc. We decided to run the accelerator at 200 Hz repetition rate, instead of the nominal 300 Hz , in order to reduce the risk of further interruptions. After the tungsten mesh moderator was replaced in June, the positron flux at the entrance to the buffer gas trap nearly doubled, then decreased by 30% by the end of the antiproton run. This is the expected behaviour, either due to contamination of the moderator surface, or due to the accumulation of lattice defects in the tungsten.

We commissioned a new positron capture system, which replaces the first stage of the Buffer Gas Trap (BGT). The original system was based on the classical "Surko trap" scheme. In the first stage, positrons were captured in the trap after an inelastic collision with a nitrogen molecule. In the new scheme, shown in Figure 2, the incoming positrons are implanted into an ultra-pure, semiconductor-grade silicon carbide (SiC) single-crystal wafer, which is placed behind the second stage of the BGT's Penning-Malmberg trap. The SiC acts as a positron remoderator: the implanted particles are re-emitted with a kinetic energy of about 3 eV well below the 50-150 eV energy range of the incoming beam. At this low energy they remain trapped. The pulse length of the primary beam was reduced from 2.5 μs to 1.5 μs by bunching via modulation of the tungsten mesh moderator voltage. Shorter pulses reduce the loss of positrons due to annihilation at the remoderator after returning from the other end of the trap.

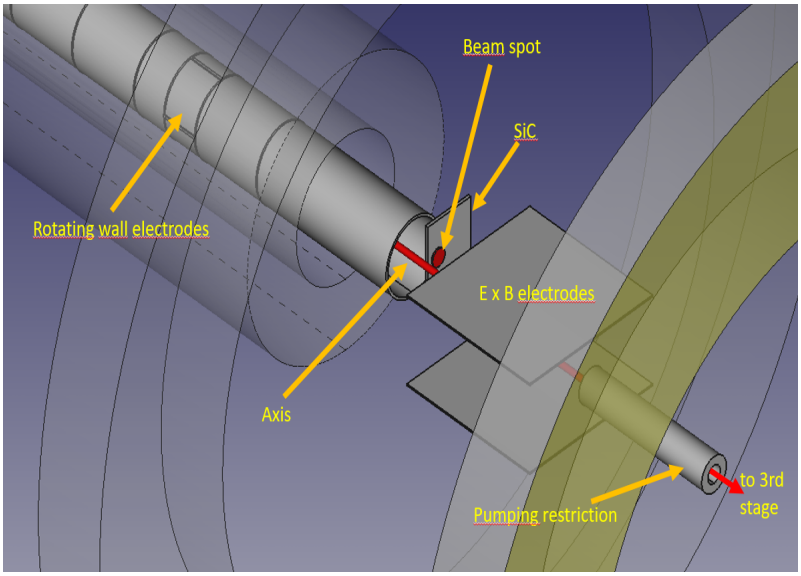

Figure 2: *The silicon carbide remoderator based trapping scheme in the buffer gas trap.*

The remoderator is located on the side about 5 mm from the axis of the trap, in order to leave the axis free when the particles are ejected towards the third stage. A steering coil directs the primary beam onto the SiC crystal ("Beam spot") in Figure 2. The trapped positrons are cooled by carbon dioxide gas and compressed on the axis of the trap by a "rotating wall"(RW) potential. In the production setting, the positrons are collected and compressed for 125 ms before being transported to the third stage through a narrow pumping restriction tube (red line in Figure 2). We have installed a new electrode stack for the first and second stage, which is better suited to the new system. The new setup has been commissioned, and the trapping efficiency in the second stage of the BGT has more than doubled, compared to the original setup.

The high field trap (HFT) was moved out of the positron beamline and the electrode stack removed. We painted the inner surfaces of the electrodes with colloidal graphite, as this treatment reportedly helps to reduce instabilities due to the "patch effect". The HFT was re-installed in the beamline at the beginning of summer 2023. As of December 2023, with the new tungsten moderator, the SiC-based accumulating scheme and some improvement of the transport between

BGT and HFT, the rate of positron accumulation in the HFT is more than three times higher than in December 2022. Up to 6×10^8 positrons are accumulated between two consecutive antiproton pulses. At the moment, however, the stacking of positrons in the HFT shows a saturation around a maximum amount of 1×10^9; work is ongoing to improve this limit.

4 Positronium production

The transport between the High Field Trap and the Reaction Chamber is a delicate issue, since the positron bunch must travel from the high magnetic field region in the trap to a low field region in the reaction chamber. After extraction from the trap, the bunch is accelerated by a pulsed drift tube (typically to 4.3 keV) to exit the field non-adiabatically. The length of this tube was increased from 300 to 380 mm in order to accommodate for longer pulses. From simulation, the transport efficiency is found to depend mainly on the radius of the bunch extracted from the trap. It is also rather sensitive to the details of the magnetic configuration and of the electrostatic optical elements of the line. In the present configuration, a significant degradation of the transport efficiency is observed for bunches with the largest number of positrons, i.e. only a 5% efficiency for 6×10^8 e^+, which would limit the number of positrons on target even if the number of positrons produced and stored in the traps is increased. In 2024, a strong effort will be dedicated to better diagnose this problem, reduce the bunch radius, and optimise the line design for a better acceptance.

In the Reaction Chamber, the positron beam is used to produce a Ps cloud, by conversion on a nanoporous silica layer. The converter used for the 2022 data taking was a flat target, but the best configuration is a small cavity (typ. $2 \times 2 \times 20$ mm) in which the Ps atoms are confined, thus increasing the Ps density by a factor of order 5 to 10 (Figure 3). In 2023 we tested such a Ps cavity, which features a silicon nitride window for the positron entry and the three opposite walls covered with Ps converter plates. Other improvements compared to 2022 are the addition of a zero - Ps reference cavity (where the three converter walls have been replaced by silicon plates) and the possibility to measure the deposited charge, and hence the number of impinging positrons, for each individual target.

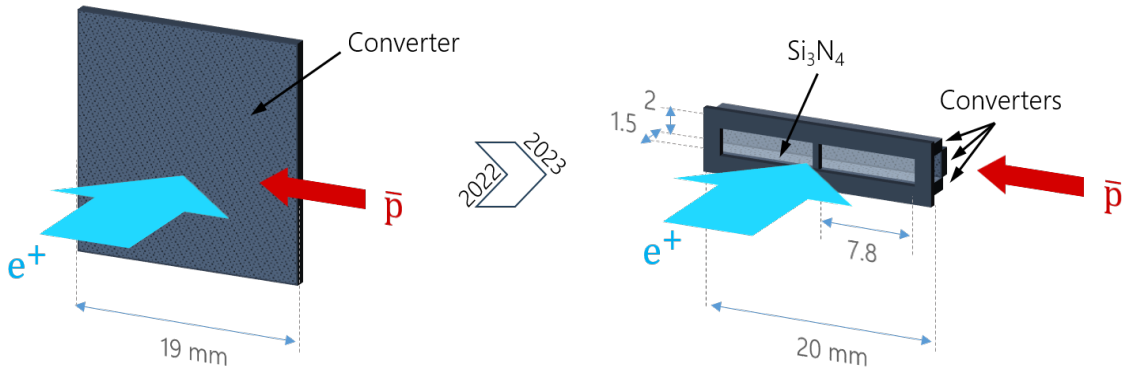

Figure 3: Schematic of the GBAR Ps converters. Left: flat target (2022); right: cavity (2023).

The detector and method used to derive the positronium fraction were described in [1]. We compare the results of the Ps cavity to those of a simpler flat converter plate. The preliminary result of the annihilation lifetime spectra analysis is that the flat converter target has a e^+ to Ps conversion yield of 24 %, while the Ps cavity produces 19 %. The difference of these two numbers is attributed to the 79% acceptance of the cavity window for the e^+ beam spot size and shape used in this study, which indicates that the Ps yield in the cavity is optimal. Furthermore, the lifetime found for the Ps in the cavity is the same as in vacuum, which shows that the Ps atoms efficiently reflect on all the walls of the cavity, as expected.

5 Antiproton beam

Figure 4 shows the configuration of the antiproton line at the end of 2023. In 2023 ELENA provided a very good 100 keV $\overline{p}$ beam with a high availability, with one bunch every two minutes approximately. The typical bunch intensity as recorded by the beam monitor was around 7×10^6 $\overline{p}$. We use a drift tube to decelerate the antiprotons to energies below 10 keV, suitable for producing

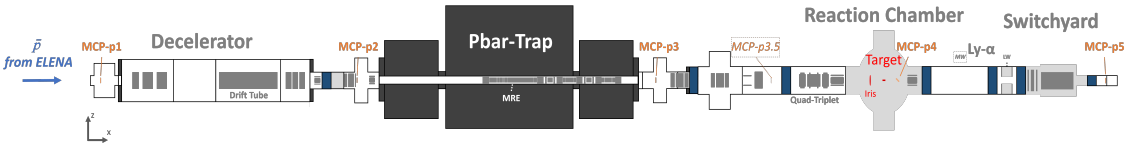

Figure 4: *GBAR $\bar{p}$ beam line end of 2023. The $\bar{p}$ beam is decelerated by the drift tube, then captured in the antiproton trap where it can be stored and cooled. Antiprotons can then be extracted and focused in the reaction chamber to meet the Ps target to form $\overline{\mathrm{H}}$ atoms. After the reaction chamber an electrostatic Switchyard(SY) can deflect the $\bar{p}$ beam to the ion beamline. For the $\overline{\mathrm{H}}$ formation experiment, the SY and additional deflectors remove the $\bar{p}$s right after the reaction region, and neutral atoms are detected in MCP-p5 located in straight line downstream.*

antihydrogen $\overline{\mathrm{H}}$ [5]. This tube is held at more than 90 kV for 3 s before the antiproton bunch arrives, and is then switched to ground in less than 30 ns while the particles are traversing it. Thanks to bunch rotation in ELENA, the bunch length was 40 ns (RMS), ensuring a complete containment inside our deceleration drift tube (DT), given also the small arrival time jitter of about 4 ns. The bunch rotation implies a doubling of the momentum spread, up to 2×10^{-3}, but this has a negligible impact for us. The horizontal and vertical emittances were unchanged with respect to 2022, i.e. 2.9 and 2.1 μm (RMS) resp . These values are about 2.5 times larger than design, with a significant impact on the decelerated beam size. In the experiment, antiprotons will now be captured and cooled by the antiproton trap, making them less dependent on the original 100 keV beam emittance. The stability and reproducibility of the $\bar{p}$ beam was excellent, from bunch to bunch and along the run period.

ELENA also enabled the delivery of 100 keV H^- ion bunches every $\approx$ 15 s, i.e. a much higher repetition rate than antiprotons. This H^- beam has proved to be very useful for a quick beam steering. However, the intensity of the H^- beam varies strongly from bunch to bunch, and the position of this beam slightly varies along the AD cycle, making it difficult to use for an accurate beam adjustment. In the coming year, we also plan to use the H^- beam for an important physics goal, see below the "SPHINX" project in section 8. As explained below, the H^- beam will be used without trapping, and a reduction of the emittance would also be very beneficial.

At the beginning of 2023, the decelerator section was opened and further improved, by removing unused electrodes, refining the DT supporting and polishing, removing neighboring ion pumps, etc. During the 2023 run, the DT was operated reliably at voltages above 90 keV (mainly 94 kV to 97 kV) with a very low leakage current (limited by that of the HV switch), ensuring a precise energy of the decelerated beam.

This procedure is described in the 2023 PhD thesis of C. Roumegou [21] which also describes a comprehensive simulation of the proton transport beamline.

During the first half of 2023, the beam line was kept as in 2022, i.e. with a simple transfer line between the decelerator and the reaction chamber, to enable further adjustments and tests, in particular with the H^- beam, testing the laser photodetachment (see below). Then in September, the antiproton trap was installed in its nominal position after the decelerator and before the reaction chamber. The first operations of this trap is described below in section 6.

6 Antiproton trap

The antiproton trap [6] is meant to constrain the decelerated antiproton beam to a smaller phase space with smaller energy and time spread. The goal is to ensure a high efficiency of passing through the Ps target cavity for antihydrogen ion production, and capturing of the produced antihydrogen ion by a precision trap downstream in the free-fall measurement section. The cooling of antiprotons in the trap is achieved by making them interact with a dense, cold, electron plasma.

Until Sep. 2023, the antiproton trap had been placed at the end of the antiproton beam line for commissioning studies. In this temporary position, the 3 operational functions which are antiproton trapping, antiproton cooling, and electron compression were demonstrated using a lower beam quality (intensity $= 2 \times 10^5$ $\bar{p}$) compared with the final position. This allowed to demonstrate an antiproton trapping efficiency of $\epsilon \sim 70\%$, and a cooling time of $\tau_c \sim 4s$ to decrease the antiproton energy below 100 eV. Regarding trapped electrons, the application of the RW technique increased the electron plasma density by a factor of 5. In Sep. 2023, the antiproton trap was moved to its nominal position, between the decelerator and reaction chamber. Four

weeks of commissioning and tests, until the end of the 2023 beam time, allowed to confirm most operational functions.

- Electron accumulation: The electron accumulation scheme was stably operated, with enough density of electron plasma for cooling antiprotons.
- Antiproton trapping: decelerated antiprotons are guided to the trap and captured by HV lenses with fast switches. Out of 8.0×10^6 antiproton flux per injection, 73% entered the trap. The trapping efficiency ($trapped\ \overline{\mathrm{p}}/injected\ \overline{\mathrm{p}} = 4.6 \times 10^6/5.8 \times 10^6$) reached 81%.
- Antiproton cooling: by interaction with cooled electrons, 3 & 6 keV antiprotons are cooled below 140 eV and trapped in the harmonic potential well in 10 sec.
- Antiproton compression: We started to study antiproton plasma compression using the RW technique. Qualitatively we observed an increase of the antiproton plasma lifetime and a decrease of the transverse size of the extracted antiproton beam, re-accelerated to 3 keV (Figure 5). Work is underway to better understand the beam shape and the plasma radial and axial size.

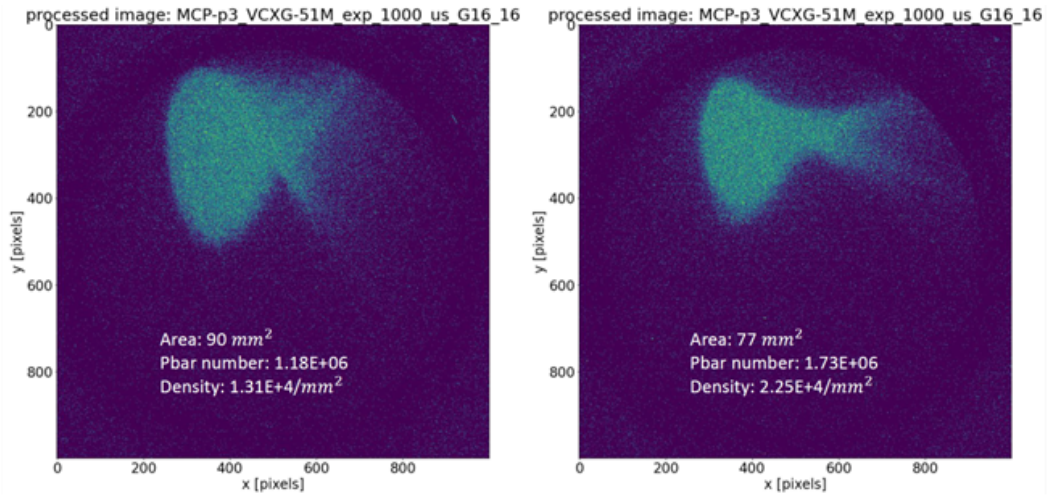

Figure 5: *Rotating Wall operation, first attempts: the extracted antiproton beam profile on MCP3 before compression(left) and after compression(right). Work is ongoing to better control the beam shape and size.*

- Antiproton extraction and bunching: the antiproton plasma is first extracted from the harmonic potential well (∼40 eV) , then accelerated by HV switching of a long electrode, still inside the high magnetic field region. The nominal accelerator lens (10cm long) had an electrical contact problem, but acceleration was nevertheless performed by a shorter lens (5cm), which limited the acceleration efficiency to 36%. A buncher scheme was tested which reduces the plasma axial size by applying a time-varying sawtooth potential, resulting in an increase of the acceleration efficiency by $40 \sim 50\%$.
- The trap could also trap H^- ions delivered by ELENA and decelerated in GBAR. However, attempts to cool them with electrons led to a quick loss of the ions.

7 Progress on the Lamb Shift experiment with antihydrogen atoms

The beam like production of antihydrogen atoms in GBAR allows for a field free determination of the antihydrogen 2S - 2P Lamb Shift (LS) [17] by detecting 2S states surviving microwave radiation applied from the outside (see Figure 6 left).

$\overline{\mathrm{H}}$ atoms in the 2S state should be copiously produced in GBAR (∼ 15% at 6 keV [7]) and can be detected by Lyman-α photons through Stark quenching in an electric field of a few 100 V/cm.

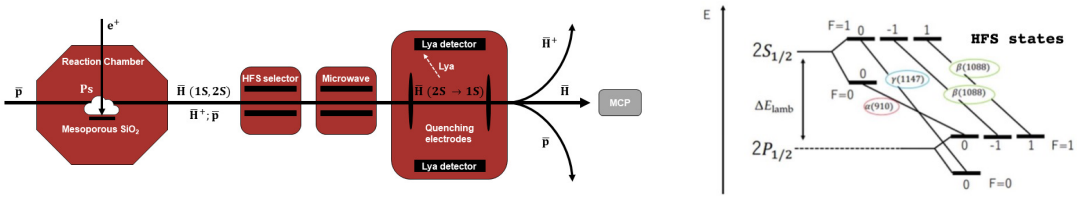

Figure 6: *Left: Arrangement of 2 microwave cavities after the target area in front of the Lyman-α detector in the GBAR experiment for the LS measurement. Right: Details of the 2S - 2P LS manifold for H.*

The detector consists of 4 CsI coated fast MCPs for a good background suppression by event timing. A 100 ppm precision in the microwave transition (at ∼1 GHz) would allow to determine the antiproton charge radius to a 10% level,[17]. The setup was initially (2020-2021) commissioned at PSI with hydrogen and muonium atoms[18], and also in 2021 in GBAR with protons and an ultra thin carbon foil [19] (see our SPSC report from Jan 2022).

The produced number of antihydrogen atoms in 2022 was too small to start searching for Lyman-α photons, but it allowed a first study of backgrounds, which, as expected, will be dominated by pions from close-by $\overline{\mathrm{p}}$ annihilations. Photons from e^+ annihilations are less critical due to a larger separation in event times.

Recently a larger vacuum chamber was installed to host new microwave cavities with a larger central bore (30 *mm* diameter, Figure 7 left) to reduce annihilations from the beam halo. Additionally a beam collimator was added to the target area. The first microwave cavity, working as a hyperfine state (HFS) selector, is designed to be resonant at around 1.1 GHz to depopulate β and γ transitions of the 2S - 2P manifold (see Figure 6 right), This will be necessary for the highest res-

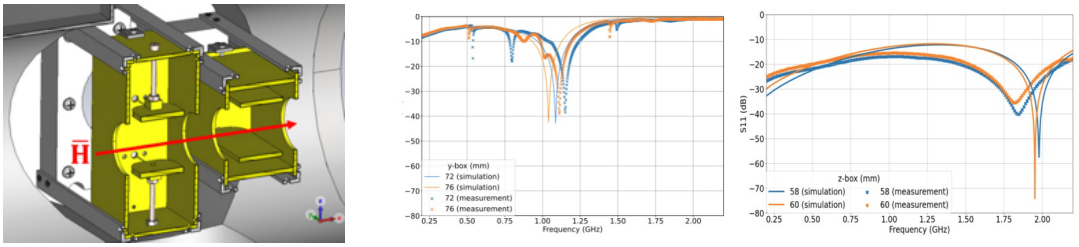

Figure 7: *Left: New microwave setup (2023) with the 2 cavities owning a larger, 30 mm, bore. Right: Comparison of measurements of the RF properties of the cavities with simulations.*

olution measurement of the (remaining) α line, once large numbers of $\overline{\mathrm{H}}$ atoms are available. The second cavity is designed to be non-resonant for better scanning linearity. The RF behaviour of the new microwave system was verified with a vector network analyser and dedicated power meters. Measurements, together with simulations for slightly different geometrical variations, are shown in Figure 7 right. Similar to the test with protons, the assembly will be evaluated with a carbon foil as soon as H^- beams are available in early 2024 under identical conditions as for antiprotons later in the year. The planned increase in $\overline{\mathrm{H}}$ production rate in 2024 should allow for a first detection of Lyman-α photons from antihydrogen atoms in GBAR. For a first LS measurement at a precision of 10 MHz, about 1000 $\overline{\mathrm{H}}$ events will be needed.

8 The SPHINX project using the ELENA H^- beam

The SPHINX project (Study of positronium-hydrogen interactions: negative hydrogen production cross sections) [13], promotes a physics application of the pulsed H^- beam provided by ELENA in between antiproton pulses. The H^- beam is decelerated down to 6 keV and focused into the GBAR positronium cavity, but right before this target, it is efficiently neutralised by a laser. The remaining charged ions are swept away by an electrostatic deflector. Thanks to this pulsed beam of neutral hydrogen atoms, it becomes possible to measure cross sections for the reaction $\mathrm{H} + \mathrm{Ps} \rightarrow \mathrm{H}^- + \mathrm{e}^+$, the charge conjugate reaction of $\overline{\mathrm{H}}^+$ formation. The cross-section of these reactions, which is key to the GBAR project, has never been measured up to now.
The integration of the neutralisation part and charge separator into the reaction chamber requires a careful design due to the tight space constraints, limited access and compatibility with the

GBAR antiproton physics program. In 2023, the mechanical design has been well advanced and the fabrication of several parts started. The installation into the reaction chamber is foreseen early 2024. Tests of metallic mirrors have been carried to enable an optimized use of the laser through multiple reflections.
Efforts were also made to find a working point for the H^- with the antiproton trap, either in passthrough mode or in trapping mode. The conclusion so far is that the passthrough mode degrades the beam quality too much while the trapping mode is inefficient, due to the impossibility of cooling the ions, as mentioned above. Without further improvement, the SPHINX project would first take the beam transmitted through the antiproton trap for commissioning, then it would mainly take data without the trap during the two months outside the antiproton beam time, provided the H^- beam remains available.
Finally, photodetachment tests were successfully carried out in the reaction chamber, with a single pass of the photodetachment laser at the position of the positronium target. As a side product, the production of a beam of H atoms provides a tool to check the trajectory and acceptance of neutrals in the GBAR antiproton / antihydrogen beamline.

9 Related projects in the collaborating institutes

- In the future, the $\overline{H}^+$ion will be cooled by sympathetic cooling with Be^+. This process is studied at LKB (ESPRIT project) with the Be^+/Sr^+ couple which features a similar mass ratio, using a segmented surface trap with two trapping zones. The transfer protocol has been tested with Sr^+ and a 95% success rate has been achieved. Characterization of the ion's kinetic energy after transfer is well underway. Development is currently focused on trapping Be^+ with Sr^+.

  The 313nm laser for cooling the Be^+ ions has been set up (sum frequency generation of 1550nm and 1050nm to obtain 626nm, then second harmonic generation in cavity to produce the 313nm beam).

- Preliminary tests will be conducted by an LKB team in the GBAR zone in the context of the PAX project (AntiProtonic Atom Spectroscopy).

- A new method of fabrication of precision ion-traps was developed at QUANTUM, Mainz, to enable an easy production of devices as designed by potential users.

10 Outlook

The data obtained during the 2022 run resulted in our first publication on antihydrogen production [1]. This is an important milestone in the GBAR programme. The production rate was low for this first attempt, thus the year 2023 was dedicated to work on increasing the fluxes of positrons and antiprotons. On the positron side, a new trapping scheme using SiC re-moderation, resulted in an accumulation of 6×10^8 e^+ between two ejections of antiprotons from ELENA, or up to 10^9 e^+ in 3 minutes, in a routine way. A new Ps cavity was built and successfully tested for Ps production. On the antiproton side a Penning-Malmberg trap was installed during the last weeks of the run, with first results on trapping, cooling and ejecting antiprotons. This late installation did not allow to try mixing for antihydrogen production. We have also demonstrated neutralisation of the H^- beam from ELENA with a laser to obtain a neutral H beam with the same parameters as the antiproton beam.

In 2024, we expect to start the run with all elements in place, increase fluxes further and steer the beams to the target location in order to produce increased numbers of antihydrogen.This would allow to measure the production cross section and to perform first tests for the measurement of the Lamb shift. We also expect to measure the cross section to produce H^- ions by interaction of H atoms with positronium, using the neutralised H^- beam from ELENA. This will allow to estimate the corresponding cross-section with incident antihydrogens to produce anti-ions.

Acknowledgements

We thank F. Butin and the EN team, L. Ponce and the AD/ELENA team for their fruitful collaboration. In particular we thank the BE department and the ELENA team for providing the H^- beam after the pbar beamtime. Thanks also to the Material, Metrology and Non-Destructive

Testing lab at CERN (EN-MME-MM) for their help, expertise and access to the metallography equipments.

References

[1] Adrich, P., Blumer, P., Caratsch, G. et al. Production of antihydrogen atoms by 6 keV antiprotons through a positronium cloud. Eur. Phys. J. C 83, 1004 (2023). https://doi.org/10.1140/epjc/s10052-023-12137-y

[2] M. Charlton et al., Nuclear Inst. and Methods in Physics Research, **A 985**, 164657 (2021).

[3] P. Blumer et al., Nuclear Inst. and Methods in Physics Research, A **1040**, 167263 (2022).

[4] A.M.M Leite et al., Journal of Physics: Conf. Series **791**, 012005 (2017).

[5] A. Husson et al., Nuclear Inst. and Methods in Physics Research, **A 1002**, 165245 (2021).

[6] Kyoung-Hun Yoo et al., JINST **17**, T10003 (2022).

[7] C.M. Rawlins et al., Physical Review **A 93**, 012709 (2016).

[8] P. Comini, P-A. Hervieux and K. Lévêque-Simon, Corrigendum: New J. Phys. **23** 029501 (2021).

[9] K. Lévêque-Simon, PhD Thesis, University of Strasbourg, France (2020); P. Comini, PhD Thesis, Université Paris VI, Pierre et Marie Curie, France (2014).

[10] G. Bendiscioli, D. Kharzeev, Riv. Nuovo Cim. **17**, 1 (1994).

[11] ESPRIT, French ANR funded project, ANR-22-CE30-0028-01.

[12] PHOTOPLUS, French ANR funded project, ANR-21-CE30-0047.

[13] SPHINX, French ANR funded project, ANR-22-CE31-0019-01.

[14] T. Yamashita et al., Phys. Rev. A **105**, 052812 (2022).

[15] O. Rousselle et al., Eur. Phys. J. D **76**, 209 (2022).

[16] L. Gershow et al., Instruments **2**, 10 (2018).

[17] P. Crivelli, D. Cooke and M. W. Heiss, Phys. Rev. **D 94**, 052008 (2016)

[18] G. Janka et al. Eur. Phys. J. C, 80 9 (2020) 804, PRL 128, 011802 (2022), Nature Comm. 7273 13 (2022)

[19] M. Gonin, R. Kallenbach and P. Bochsler, Review of Scientific Instruments **65**, 648 (1994)

[20] AD-7/GBAR status report for the 2023 CERN SPSC, CERN-SPSC-2023-008; SPSC-SR-324

[21] C Roumegou, CERN-THESIS-2023-274; 2023UPASP093